# Original Article Enhanced glycolysis induced by activation of AKT/NF-kB signaling pathway

contributes to doxorubicin resistance in DLBCL

Yong Wu<sup>1</sup>, Zi-Jian Li<sup>2</sup>, Ming Li<sup>2</sup>, Meng Wang<sup>3</sup>, Qi-Yu Feng<sup>4</sup>, Ya-Ming Xi<sup>2</sup>

<sup>1</sup>The First Clinical Medical College of Lanzhou University, Lanzhou 730000, Gansu, P. R. China; <sup>2</sup>Department of Hematology, The First Hospital of Lanzhou University, Lanzhou 730000, Gansu, P. R. China; <sup>3</sup>Department of Hematology, The First Affiliated Hospital of Bengbu Medical College, Bengbu 233004, Anhui, P. R. China; <sup>4</sup>Cancer Research Center, The First Affiliated Hospital of USTC, Division of Life Sciences and Medicine, University of Science and Technology of China, Hefei 230036, Anhui, P. R. China

Received March 14, 2025; Accepted August 28, 2025; Epub September 15, 2025; Published September 30, 2025

Abstract: Diffuse large B-cell lymphoma (DLBCL), the most prevalent form of lymphoma, is characterized by marked tumor heterogeneity. Treatment failure in DLBCL is often driven by drug resistance, particularly to doxorubicin, and our clinical observations suggest that comorbid type 2 diabetes further increases the incidence of such resistance. However, the intrinsic mechanisms by which altered glucose metabolism modulates doxorubicin resistance in DLBCL cells remain unclear. Here, we demonstrate that aberrant glucose metabolism activates the Protein Kinase B (AKT) signaling pathway, which in turn amplifies Nuclear Factor-kappa B (NF-kB) signaling, thereby promoting doxorubicin resistance. Comparative analyses of sensitive, primary-resistant, and acquired-resistant DLBCL cell lines revealed distinct functional and pathway alterations, notably in AKT and NF-kB signaling. Experimental validation confirmed that both pathways are critical mediators of resistance: enhanced AKT activity drives downstream NF-kB activation, which boosts glycolytic capacity and enables cancer cells to survive under chemotherapeutic stress. These findings not only elucidate a metabolic mechanism of drug resistance in DLBCL but also identify AKT and NF-kB as promising therapeutic targets for overcoming both primary and acquired doxorubicin resistance.

Keywords: DLBCL, doxorubicin resistance, type 2 diabetes, glycemic metabolism, AKT/NF-kB signaling pathway

### Introduction

Diffuse large B-cell lymphoma (DLBCL) is the most common subtype of non-Hodgkin's lymphoma, accounting for approximately 30%-40% of all cases [1]. First-line therapy consists of R-CHOP immunochemotherapy - rituximab, cyclophosphamide, doxorubicin, vincristine, and prednisone - which achieves favorable responses in the majority of patients [2]. Nevertheless, up to 40% of individuals develop either primary or acquired resistance, driven by genetic alterations, adaptive signaling changes, or extended exposure to the same regimen [3, 4]. Among R-CHOP components, resistance to doxorubicin is the chief contributor to treatment failure [5] and alternative strategies such as high-dose chemotherapy or autologous

stem-cell transplantation have yielded only modest survival benefits [6].

The mechanisms underlying R-CHOP resistance are highly complex, reflecting tumor heterogeneity, drug-induced genetic remodeling, and hyperactive signaling networks [7-9]. Emerging evidence implicates metabolic reprogramming - particularly enhanced glycolysis - in mediating chemoresistance [10-12]. For example, upregulation of hexokinase 2 (HK2) augments glycolytic flux and confers therapy resistance in DLBCL [13], while activation of the non-canonical Nuclear Factor-kappa B (NF-κB) pathway promotes resistance via glycolysis modulation [14]. Therapeutically, the monocarboxylate transporter inhibitor AZD3965 synergizes with doxorubicin to overcome resistance by disrupt-

ing lactate export [15]. These studies underscore the critical interplay between altered metabolism and drug resistance in DLBCL.

Type 2 diabetes mellitus (T2DM) - characterized by impaired insulin secretion or action and systemic hyperglycemia - affects hundreds of millions globally and exacerbates numerous comorbidities [16-19]. Epidemiological and preclinical data link T2DM to increased tumor drug resistance [20-22], a finding that aligns with our observation of higher doxorubicin resistance rates in DLBCL patients with concomitant T2DM. Central metabolic regulators in T2DM include the Adenosine Monophosphateactivated Protein Kinase (AMPK) and Protein Kinase B (AKT) pathways, whose modulation profoundly influences cellular energy homeostasis [23-31]. Notably, AKT signaling interfaces with the NF-kB pathway to govern apoptosis and survival in cancer cells [32-34]. However, whether T2DM-associated metabolic alterations drive chemoresistance in DLBCL via the AMPK/AKT axis has not been elucidated.

In this study, we retrospectively analyzed 235 DLBCL patients - 69 with T2DM and 166 without - and confirmed a significantly higher incidence of doxorubicin resistance among those with T2DM. By generating primary-resistant and acquired-resistant DLBCL cell lines and performing transcriptomic profiling, we identified AKT-centered metabolic pathways as markedly enriched in resistant cells. Functional assays, including Seahorse metabolic flux analysis, validated heightened glycolytic activity and confirmed AKT and NF-kB pathway activation in resistant lines. Pharmacological inhibition of AKT attenuated NF-kB signaling and restored doxorubicin sensitivity in vitro, and combined AKT/NF-kB blockade suppressed tumor growth in vivo. Together, our findings reveal a mechanistic link between glucose metabolism, AKT/NF-kB signaling, and doxorubicin resistance in DLBCL, and suggest novel therapeutic targets to overcome both primary and acquired chemoresistance.

### Materials and methods

Patient recruitment and clinical study

A total of 235 DLBCL patients were retrospectively collected from the First Hospital of Lanzhou University and the First Affiliated

Hospital of Bengbu Medical College from 2016 to 2022. All participants provided informed consent prior to the study. The main diagnoses of these patients were whether DLBCL was associated with drug resistance. Patients over 80 years old or less than 18 years old and those who did not meet the inclusion criteria were excluded. All patients received at least 3 R-CHOP treatment courses. Response categories including Complete Response (CR), Partial Response (PR), Stable Disease (SD), and Progression Disease (PD) were defined according to the Lugano 2014 classification. Resistance was categorized as primary if PD occurred during or within 3 cycles after treatment, or secondary if PD emerged after initial CR/PR. All imaging assessments were performed by two independent radiologists blinded to clinical data. Their medical histories and blood test indicators, including gender, age, Body Mass Index (BMI), β2-microglobulin (β2MG), International Prognostic Index score (IPI\_score), cholesterol (CHO), triglyceride (TG), C-reactive protein (CRP), Erythrocyte Sedimentation Rate (ESR), stage, molecular subtype, history of T2DM, were collected. Relevant hematoxylin and eosin (H&E) staining and immunohistochemical staining were performed on archived specimens.

### Reagents

Phosphorylated AKT, AKT, phosphorylated AMPK, and AMPK antibodies are from Abcam in the United States. The NF-kB antibody is from Biyuntian Company in China. Doxorubicin, MK2206 for the AKT pathway, and Bortezomib for the NF-kB pathway were purchased from Selleck.cn in Shanghai, China. The Cell Count Kit-8 reagent was purchased from Biyuntian Company. The apoptosis assay kit was purchased from Biosharp Company. The glycolysis assay kit was purchased from Agilent in Shanghai, China. B-cell lymphoma 2 (Bcl-2), Myeloid cell leukemia 1 (Mcl-1), B-cell lymphoma-extra large (Bcl-xl) antibodies are from Biyuntian Company in China.

### Cell proliferation assay

According to the manufacturer's instructions, the cell proliferation assays were performed using Cell Counting Kit-8 (CCK-8; Beyotime Biotechnology, Shanghai, China). Briefly, cells were seeded into a 96-well plate at a density of

 $5{\times}10^3$  cells per well. After the cells were treated or cultured for a certain period, 10  $\mu L$  of CCK-8 solution was added and mixed well. After incubating for 1 hour at 37°C in a CO $_2$  incubator, the absorbance at 450 nm was measured using Synergy H1 (Biotek, Agilent, California, USA). The drug inhibition rate of cancer cells and the corresponding half-inhibitory concentration (IC $_{50}$ ) value were calculated based on the absorbance reading.

# Cell apoptosis assay

After processing, all cells were collected in EP tubes and washed with PBS before being added to the incubation fluid. Apoptosis was evaluated using the apoptosis detection kit (Biosharp, 15900455, China) by staining the cells with 5  $\mu L$  of Annexin V-FITC/PI staining reagents for 15 minutes. After staining, the cells were washed three times and analyzed for apoptosis using a flow cytometer. The apoptotic ratio of the cells was analyzed using FlowJo software.

# High-throughput RNA-seq analysis

Tissue samples were subjected to high-throughput RNA sequencing analysis at EnergyCorp. Total RNA was extracted using Trizol (Invitrogen, USA). The concentration and integrity of the RNA were assessed using Qubit® 2.0 (Life Technologies, USA) and Agilent 2200 TapeStation (Agilent Technologies, USA), respectively. Following the manufacturer's instructions, small RNA libraries were prepared using the NEB-Next® Multiplex Small RNA Library Prep Set (NEB, USA) from 1 µg of total RNA from each sample. Subsequently, sequencing was performed on the HiSeq 2500 platform (Illumina, USA) using the single-end 50 bp protocol provided by Generey (China), a subsidiary of EnergyCorp.

# Cell culture

The DLBCL cell lines OCILY19, OCILY3, SUD-HL6, SUDHL8, DOHH2, and normal B cell line GM12878 have been confirmed to be free of mycoplasma contamination and are cultured in high-glucose medium containing serum. The cells exhibit suspension growth and are maintained in a 37°C incubator with 5% carbon dioxide. The culture medium is replaced every 2 days, and when the cells reach 80% con-

fluency, they are subcultured and further processed for subsequent experiments.

Cultivation of acquired doxorubicin-resistant DLBCL cell lines

SUDHL8S cells, which are initially sensitive to doxorubicin and in a good state, were repeatedly cultured and gradually exposed to increasing concentrations of doxorubicin. This process continued until the IC $_{50}$  of doxorubicin reached 0.2  $\mu$ M, indicating the development of doxorubicin-resistant SUDHL8R cells. The acquired doxorubicin resistance of SUDHL8R cells was subsequently confirmed through validation.

### Western blot

The cell tissue was lysed using RIPA lysis buffer (Beyotime Biotechnology, China). The protein concentration was measured using the BCA protein assay kit (Beijing Biological Technology, China). Forty micrograms of protein were separated on a 10% SDS-PAGE gel and then transferred onto an NC membrane (EMD Millipore). After transfer, the membrane was blocked with 5% bovine serum albumin and washed three times with PBS. Subsequently, the membrane was incubated with the primary antibody overnight at 4°C. After washing with PBS, the membrane was incubated with the H&L secondary antibody for 1 hour at 25°C. Protein bands were visualized using an ECL substrate kit (Thermofisher). Semi-quantitative analysis of protein expression levels was performed using Image-Pro Plus software (version 6.0; Media Cybernetics).

# Hematoxylin and eosin staining

The tissue was fixed in 4% paraformaldehyde, embedded in paraffin, and then sectioned into 5  $\mu$ m thick slices. Subsequently, these tissue sections were stained with H&E.

## *Immunohistochemistry*

The paraffin sections of the tissue were deparaffinized and rehydrated using xylene and ethanol, respectively. To block endogenous peroxidase, the sections were then incubated with 3% hydrogen peroxide solution. Antigen retrieval was performed using a 0.1 M sodium citrate buffer (pH 6.0) for 60 minutes. Subsequently, the sections were incubated with 5% BSA for 1

hour, followed by incubation with the primary antibody at room temperature for 4 hours. Then, a secondary antibody conjugated with horseradish peroxidase (HRP) from Abcam (Cambridge, UK) was applied and incubated at 37°C for 1 hour. The sections were washed twice with PBS for 5 minutes each, followed by staining with 3,3'-Diaminobenzidine (DAB) and counterstained with hematoxylin. These images were captured using an optical microscope (Olympus-IX73-DP80, Japan). Positive staining appeared as brownish-yellow color.

### Seahorse assay

According to the manufacturer's guidelines, the Seahorse XF Glycolysis Stress Test Kit (Seahorse Bioscience, Cat #: 103020-100), Seahorse XF Cell Mito Stress Test Kit (Seahorse Bioscience, Cat #: 103015-100) and Seahorse XF Real-Time ATP Rate Assay Kit (Seahorse Bioscience, Cat #: 103592-100) are used to evaluate extracellular acidification rate oxidative mitochondrial pressure and ATP production rate of cells. Cells are seeded at a density of 8000 to 20000 cells per well in a 96well Seahorse assay plate coated with poly-Dlysine. After different treatments, the cells are incubated for 30 minutes at 37°C in an unbuffered DMEM medium in a non-CO<sub>2</sub> incubator. Then, at specified time points, the cells are treated with respective reagents. Glucose Uptake Assay Kit (Merck Life Sciences, Cat #: MAK542) was used to detect the glucose uptake of cells.

### Animal experiments

Female BALB/c Nude mice were adaptively grown in cages for one week, followed by subcutaneous injection of tumor masses. SUDHL8R cells were diluted to a concentration of 5×10<sup>7</sup>/ml. Then, 100 ul of cell suspension was mixed with matrix gel and injected into the armpit of the mice. After 3 weeks of growth, when the tumor volume reached approximately 100 mm<sup>3</sup>, drug intervention was administered. The control group received physiological saline, while the Dox group received doxorubicin chemotherapy. In the Dox + AKT inhibition group, AKT signaling pathway was inhibited along with doxorubicin chemotherapy based on body weight. Similarly, in the Dox + NF-kB inhibition group, NF-kB signaling pathway was inhibited along with doxorubicin chemotherapy based on body weight. The treatment cycle lasted for 10 days, during which the body weight and subcutaneous tumor volume of the mice were recorded. 10 days later, euthanize the mice by  ${\rm CO}_2$  inhalation followed by cervical dislocation, and collect the specimens. After 10 days, the mice were euthanized and specimens were collected. The specimens were either immersed in 4% paraformal dehyde or placed in a -80°C refrigerator.

# Statistical methods

Univariable logistic analysis or multivariate logistic analysis analyzed using R language. Statistical analysis was performed using SPSS 21.0. Continuous variables are expressed as mean  $\pm$  standard deviation (SD). Independent samples t-test was used to compare two independent groups, and repeated measures ANOVA was applied to the repeated data. Categorical variables are presented as counts or percentages, with the  $\chi^2$  test used for group comparisons. A p-value of less than 0.05 was considered statistically significant.

### Result

Higher R-CHOP treatment resistance rate in DLBCL patients with T2DM

To analyze the interfering factors of resistance, this study conducted Univariable Logistic and Multivariate Logistic Analysis on the characteristics of resistant and non-resistant groups. The results of the Univariable Logistic Analysis revealed that age, CRP, B2MG, ESR, IPI score, Molecular Subtype, and the presence of a history of T2DM were significant confounding factors for R-CHOP resistance (all P<0.05, Table 1). In the Multivariate Logistic Analysis, the presence of a history of T2DM was identified as one of the influencing factors for R-CHOP resistance (P<0.001, Table 1). To determine whether T2DM-associated metabolic disturbances influence R-CHOP resistance in DLBCL, we performed a retrospective analysis of 235 patients, stratifying them into four cohorts by diabetic status and treatment response (Figure 1A). Baseline characteristics - including sex, age, and BMI - were comparable across all groups (all P>0.05, Table 2). H&E and immunohistochemical staining of diagnostic biopsy specimens confirmed DLBCL in each cohort (Figures 1B, S1). When comparing diabetic ver-

**Table 1.** Analysis of factors related to drug resistance and non-drug resistance

Characteristics	Univariable Logisti	ic Analysis	Multivariate Logistic Analysis		
Characteristics	OR (95%)	Р	OR (95%)	Р	
Gender (n, %)					
Female	ref				
Male	2.0 (1.11-3.62)	0.021	2.02 (0.97-4.22)	0.06	
Age (year)	1.01 (0.99-1.04)	0.268			
BMI	1.03 (1.00-1.06)	0.068			
CRP (mg/L)	1.04 (1.03-1.06)	< 0.001	1.04 (1.02-1.06)	< 0.001	
β2MG (mg/L)	1.22 (1.01-1.47)	0.039			
ESR (mm/h)	1.05 (1.03-1.06)	< 0.001	1.03 (1.01-1.05)	0.001	
CHO (nmol/L)	0.88 (0.63-1.22)	0.435			
TG (nmol/L)	0.98 (0.71-1.34)	0.893			
IPI_score (n, %)					
0-2	ref		ref		
3-5	1.54 (1.02-2.33)	0.041	1.47 (0.88-2.45)	0.14	
Stage (n, %)					
1	ref				
II	1.48 (0.39-5.52)	0.563			
III	1.36 (0.33-5.67)	0.671			
IV	2.36 (0.59-9.39)	0.222			
T2DM (n, %)					
No	ref		ref		
Yes	4.59 (2.47-8.53)	< 0.001	4.76 (2.24-10.11)	<0.001	
Molecular Subtype (n, %)					
GCB	ref				
non_GCB	2.67 (1.49-4.80)	0.001			

CRP, C-reactive protein; β2MG, β2-microglobulin; ESR, Erythrocyte Sedimentation Rate; CHO, cholesterol; TG, triglyceride; IPI\_score, International Prognostic Index score; T2DM, Type 2 Diabetes Mellitus; GCB, germinal center B-cell-like.

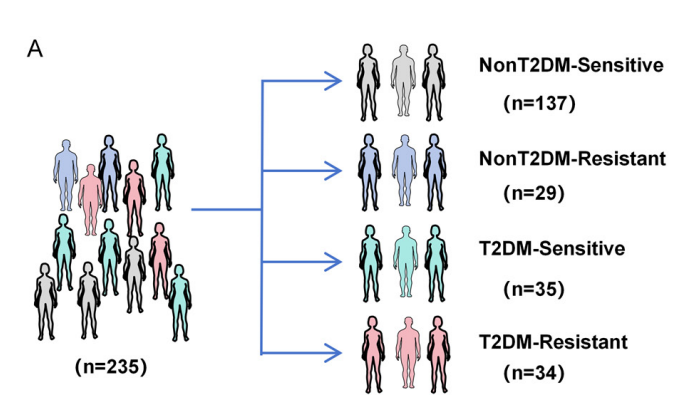


Figure 1. DLBCL patients with concomitant T2DM have a higher drug resistance rate. A. Workflow diagram for clinical data collection. B. H&E staining results of tissue specimens from the four groups of patients (×200).

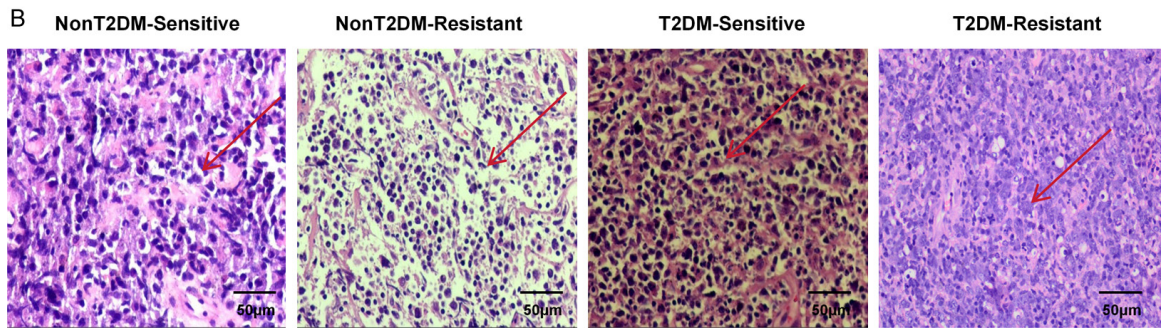


Table 2. The demographics and clinical characteristics of individuals

	NonT2DM-Senstive (n=137)	NonT2DM-Resistant (n=29)	T2DM-Sensitive (n=35)	T2DM-Resistant (n=34)	P Value
Female/Male	76/61	10/19	19/16	12/21	0.07
Mean age	57.24 ± 12.98	58.71 ± 13.41	56.63 ± 12.62	61.78 ± 12.60	0.13
BMI	24.69 ± 4.14	23.95 ± 3.75	25.63 ±3.80	24.10 ± 3.83	0.37

Table 3. The clinical treatment resistance rate

	NonT2DM	T2DM
Sensitive	137	35
Resistant	29	34
Drug resistance rate	17.47%	49.27%

sus non-diabetic patients, the T2DM group exhibited a significantly higher R-CHOP resistance rate (49.27% vs. 17.47%; *P*<0.05, **Table 3**). These results suggest that aberrant glucose metabolism in T2DM may contribute to increased R-CHOP treatment resistance in DLBCL.

Primitive resistant cells possess unique genomic traits that contribute to their differential drug resistance

We next evaluated doxorubicin sensitivity across a panel of DLBCL cell lines and the normal B-cell line GM12878. Based on IC $_{50}$  values, OCI-LY19, DOHH2, and SUDHL8 were classified as sensitive, whereas OCI-LY3 and SUDHL6 were designated resistant (P<0.05, **Figures 2A**, **2B**, <u>S2A</u>). Flow cytometric analysis of apoptosis following doxorubicin treatment corroborated these classifications (\*P<0.05, **Figures 2C**, <u>S2B</u>), and immunoblotting of apoptosis markers showed markedly higher expression in resistant lines (OCI-LY3, SUDHL6) compared to sensitive lines (OCI-LY19, DOHH2, SUDHL8).

To uncover transcriptional programs underlying resistance, we performed RNA-seq on the sensitive SUDHL8 and resistant OCI-LY3 lines, confirming high-quality RNA inputs (Figure S3A). Differential expression analysis identified 5,283 genes (Figure 2D, 2E), many of which clustered within common gene families (Figure S3B, S3C). Gene Ontology enrichment highlighted pronounced alterations in metabolic processes, cellular components, and molecular functions (Figure 2F). KEGG pathway analysis further revealed significant enrichment of the AKT and NF-κB signaling axes in resistant cells

(**Figure 2G**). These data implicate metabolic and pro-survival pathways, particularly AKT and NF-κB, in doxorubicin resistance in DLBCL.

Cells with acquired resistance to Doxorubicin exhibit partially overlapping but distinct mechanisms of resistance

To explore the mechanisms underpinning acquired doxorubicin resistance, we generated a resistant derivative of the sensitive SUDHL8 line (termed SUDHL8R) by stepwise escalation of doxorubicin exposure until cells proliferated robustly at 200 nM (Figure 3A). SUDHL8R displayed a 6-7-fold increase in IC<sub>50</sub> relative to parental SUDHL8 (SUDHL8S) (Figure 3B), and flow cytometry confirmed a markedly lower apoptosis rate in SUDHL8R following doxorubicin treatment (\*P<0.05, Figure S4A). Consistently, apoptotic marker expression was substantially elevated in SUDHL8R versus SUDHL8S after drug exposure (Figure S4B), validating successful induction of resistance.

Transcriptomic profiling of SUDHL8S and SUDHL8R (QC metrics in <u>Figure S5A</u>) identified 2,628 differentially expressed genes (560 downregulated, 2,068 upregulated; **Figure 3C**, **3D**), which clustered into functional gene families (<u>Figure S5B</u>, <u>S5C</u>). Gene Ontology enrichment revealed significant involvement of immune response, vesicle localization, and DNA damage processes - the latter correlating with doxorubicin sensitivity (**Figure 3E**). KEGG pathway analysis highlighted pronounced activation of both AKT and NF-kB signaling in SUDHL8R (**Figure 3F**), implicating these axes as common drivers of primary and acquired resistance in DLBCL.

Abnormal glycolysis induced by AKT-mediated activation of the NF-kB pathway leads to the development of drug resistance

To uncover shared drivers of primary and acquired doxorubicin resistance, we intersect-

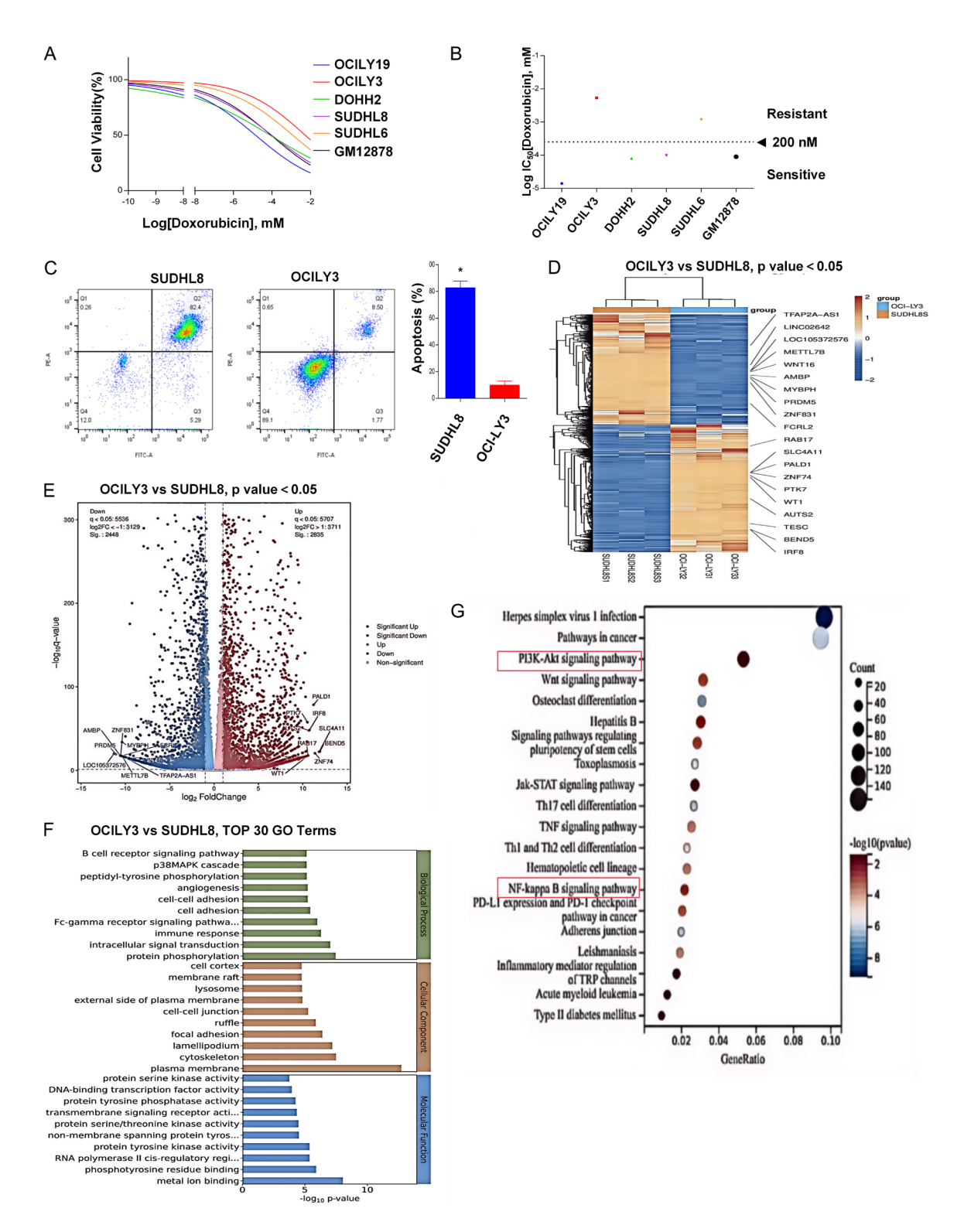


**Figure 2.** Omics results indicate significant differences in biological functions and pathway enrichment between the original resistant and sensitive cells. A. Differential sensitivity to Doxorubicin in different DLBCL cell lines. B. Cells were divided into Doxorubicin-resistant and Doxorubicin-sensitive cells based on an IC<sub>50</sub> of 200 nM. C. Apoptosis rate of sensitive cell line SUDHL8 and resistant cell line OCILY3 after 24 h of Doxorubicin treatment, \*P<0.05. D. Heatmap of differentially expressed genes identified in SUDHL8 and OCILY3 cells. E. Volcano plot of differentially expressed genes identified in SUDHL8 and OCILY3 cells. F. Analysis of biological functions of differentially expressed genes using GO Terms. G. Pathway enrichment (KEGG) analysis of differentially expressed genes.

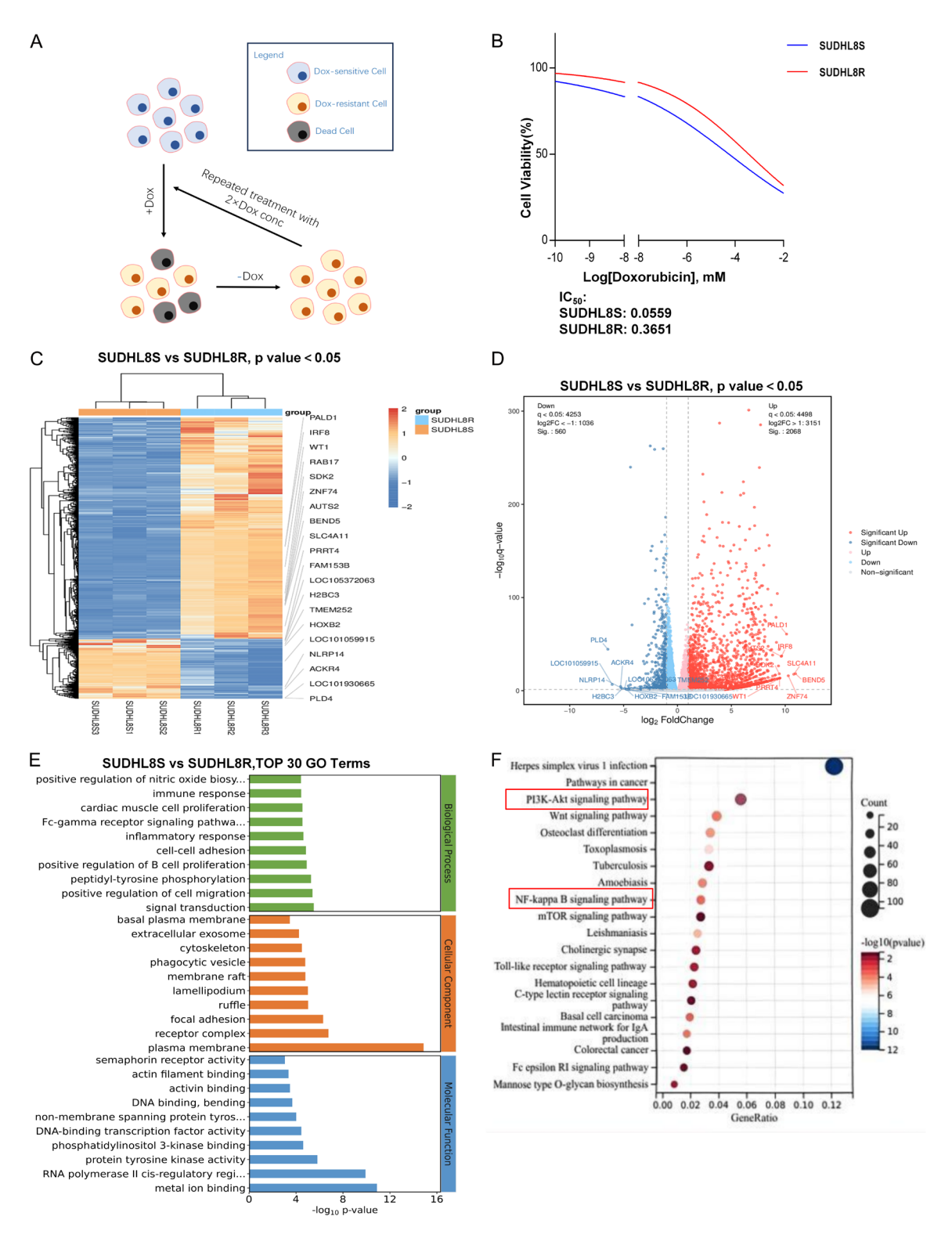


Figure 3. Omics results indicate significant enrichment differences in biological functions and pathways between induced resistant and sensitive cells. A. Induction pattern of resistant cells SUDHL8R. B. IC50 detection of induced resistant cells SUDHL8R and sensitive cells SUDHL8S. C. Heatmap of differential genes obtained from omics analysis of sensitive cells SUDHL8 and induced resistant cells SUDHL8R. D. Volcano plot of differential genes. E. Gene ontology (GO) plot of differential genes. F. Kyoto Encyclopedia of Genes and Genomes (KEGG) pathway enrichment plot of differential genes.

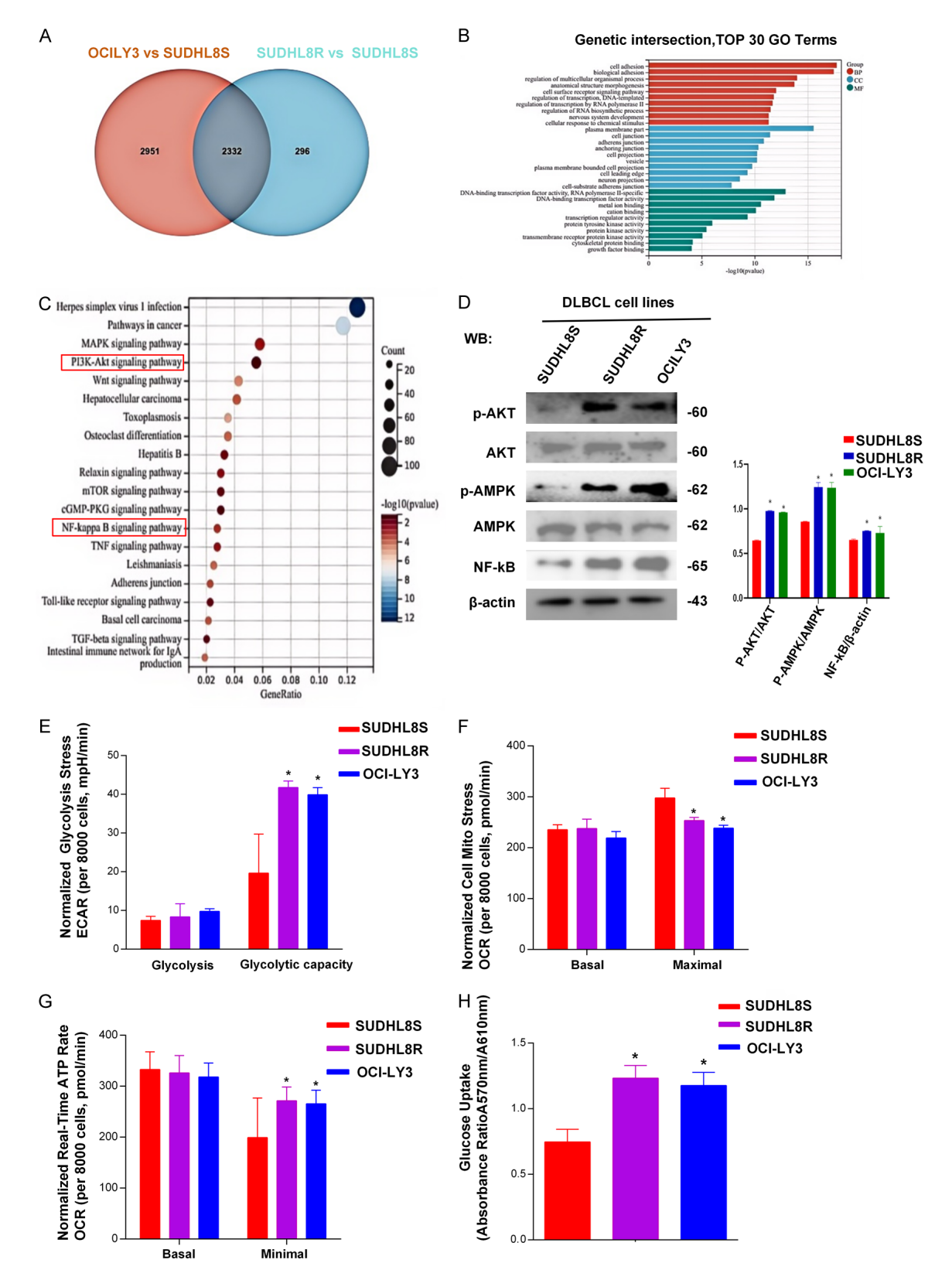


Figure 4. The AKT and NF-kB signaling pathways are abnormally activated in drug-resistant cells. A. Venn diagram showing the intersection of differentially expressed genes in two groups. B. Functional analysis of gene ontology (GO terms) for the intersecting genes. C. Enrichment pathway (KEGG) analysis of the intersecting genes. D. Abnormal activation of the internal AKT, AMPK, and NF-kB signaling pathways in the original drug-resistant cell line OCILY3

and the induced drug-resistant cell line SUDHL8R compared to the sensitive cell line SUDHL8S. Compared to the SUDHL8S group, \*P<0.05. E. Increased glycolysis stress ECAR in the original drug-resistant cell line OCILY3 and the induced drug-resistant cell line SUDHL8R compared to the sensitive cell line SUDHL8S, indicating enhanced glycolytic capacity, \*P<0.05. ECAR (Extracellular Acidification Rate). F. Decreased cell mitochondrial stress OCR in the original drug-resistant cell line OCILY3 and the induced drug-resistant cell line SUDHL8R compared to the sensitive cell line SUDHL8S, indicating lower cellular mitochondrial stress, \*P<0.05. OCR (Oxygen Consumption Rate). G. Increased Real-Time ATP Rate OCR in the original drug-resistant cell line OCILY3 and the induced drug-resistant cell line SUDHL8R compared to the sensitive cell line SUDHL8S, indicating enhanced rate of ATP generation, \*P<0.05. H. SUDHL8R and OCI-LY3 drug-resistant cells exhibit higher glucose uptake capacity compared to the sensitive cell SUDHL8S. \*P<0.05.

ed the differentially expressed genes from both transcriptomic analyses, yielding 2,332 common candidates (**Figure 4A**). Functional annotation revealed enrichment in processes such as cell adhesion, DNA-binding transcription factor activity, and RNA polymerase II - specific functions (**Figure 4B**), all of which may contribute to chemoresistance. Pathway analysis again highlighted the AKT and NF-κB axes (**Figure 4C**), supporting the hypothesis that AKT signaling regulates NF-κB in this context.

We next validated activation of the AKT, AMPK, and NF-kB pathways in the sensitive line (SUDHL8S), a primary-resistant line (OCI-LY3), and the acquired-resistant derivative (SU-DHL8R). Both resistant lines exhibited increased phosphorylation of AKT and AMPK alongside elevated NF-kB protein levels, confirming pathway activation (\*P<0.05, **Figure 4D**). Moreover, Seahorse metabolic flux analysis showed that extracellular acidification rates (ECAR) - a proxy for glycolytic capacity - were significantly higher in OCI-LY3 and SUDHL8R compared to SUDHL8S (\*P<0.05, Figures 4E, S6A). Meanwhile, the mitochondrial stress cell oxygen consumption rate (OCR) was lower in OCI-LY3 and SUDHL8R cells (\*P<0.05, Figures 4F, S6B), while their ATP production rate OCR values were higher during ATP generation demands (\*P<0.05, Figures 4G, S6C). Further studies determined the glucose uptake capacity of the three groups of cells, and it was found that the drug-resistant OCI-LY3 and SUDHL8R cells took up more glucose compared to the sensitive SUDHL8S cells (\*P<0.05, Figure 4H). Therefore, both primary and acquired drug resistance are associated with the synergistic activation of the AKT/AMPK-NF-kB signaling pathway, leading to enhanced cellular glycolytic capacity, lower oxygen consumption under stress conditions, and increased rate of ATP production during ATP demands.

Inhibition of the AKT/NF-kB signaling pathway axis transforms drug-resistant cells into sensitive cells

Treatment of the acquired-resistant SUDHL8R cells with an AKT-specific inhibitor markedly reduced phospho-AKT levels (\*P<0.05, Figures 5A, S7A, lane 4 vs. 3), confirming effective pathway blockade. Similarly, NF-κB inhibition suppressed downstream NF-κB signaling (\*P<0.05, \*\*P<0.01, lane 5 vs. 3). Notably, doxorubicin exposure alone elevated AMPK phosphorylation in SUDHL8R cells (lane 3 vs. 1), suggesting a metabolic stress response, whereas NF-κB inhibition had no appreciable effect on either AKT or AMPK activation.

Functionally, combining either AKT or NF-kB inhibitors with doxorubicin abrogated antiapoptotic protein expression and significantly increased apoptosis in SUDHL8R cells, as measured by flow cytometry (Figures 5B, S7B, S7C). Concordantly, Seahorse XF analysis showed that both drugs significantly reduced the extracellular acidification rate - an indicator of glycolytic flux - in SUDHL8R cells (\*P<0.05, Figures 5C, S6D), while enhancing the oxygen consumption under mitochondrial stress conditions and inhibiting the rate of ATP production (\*P<0.05, Figures 5D, 5E, S6E, S6F). Importantly, further research revealed that both drugs blocked the rapid glucose uptake capacity in SUDHL8R cells due to drug resistance, thereby reducing the sugar absorption in drug-resistant cells (\*P<0.05, Figure 5F).

Together, these results demonstrate that targeting AKT and NF-kB signaling not only impairs survival pathways but also suppresses the enhanced glycolysis, reduction in oxygen consumption under stress conditions and enhancement of ATP generation rate characteristic of doxorubicin-resistant DLBCL cells, thereby reversing chemoresistance.

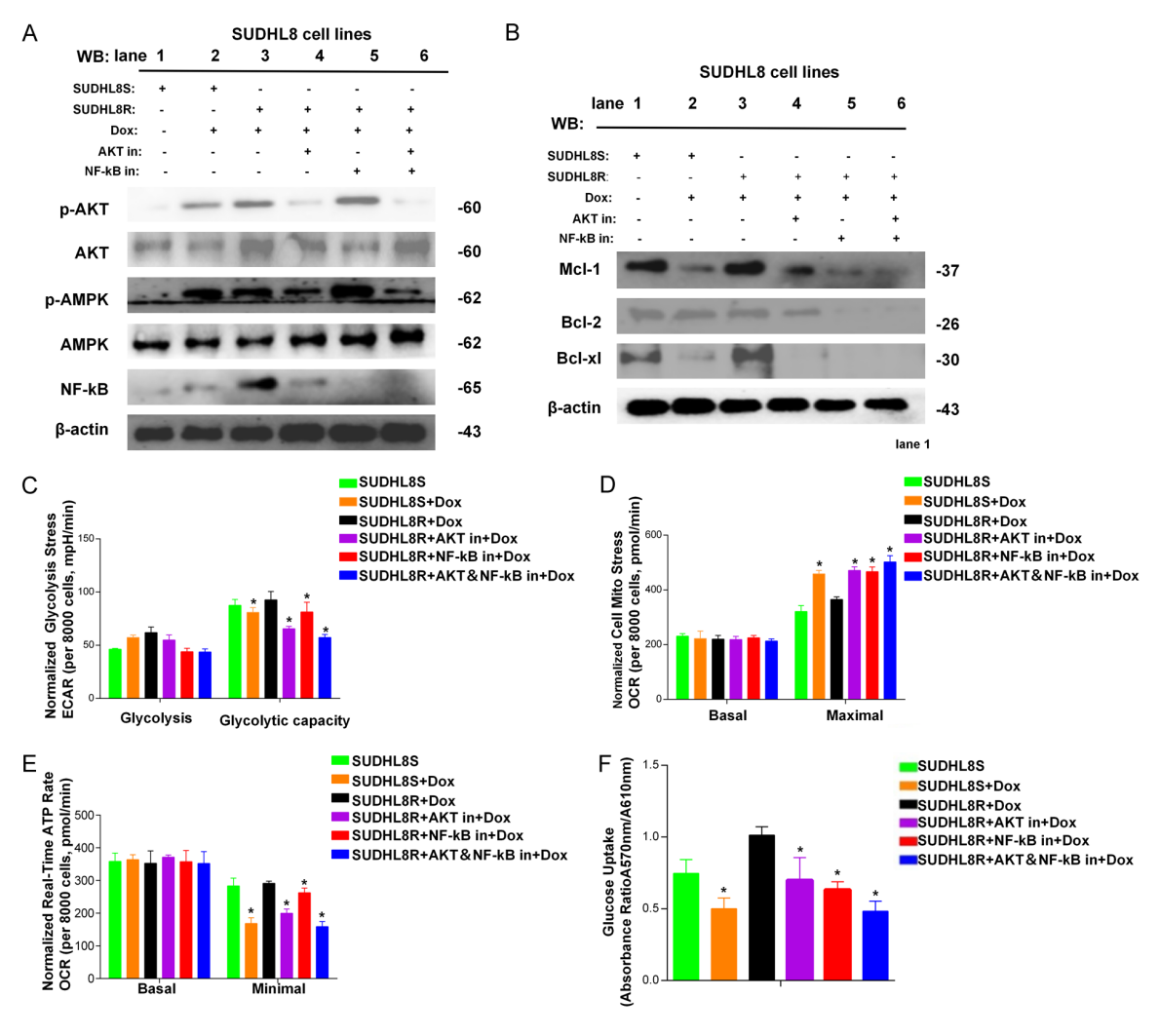


Figure 5. Inhibition of the AKT/NF-κB signaling pathway axis can reverse drug resistance in DLBCL cells. (A) Western Blot detection of the protein expression levels of AKT, AMPK, and NF-κB signaling pathways after the addition of different inhibitor. After the addition of inhibitor for AKT, the downstream NF-κB signaling pathway is inhibited, while the AMPK pathway is activated. After the addition of inhibitor for the NF-κB signaling pathway, the NF-κB signaling pathway is suppressed, and there are no changes in the upstream AKT signaling pathway and AMPK signaling pathway. (B) Western Blot detection of the expression of anti-apoptotic molecules after the addition of different drugs. (C) Seahorse XF energy detector to measure the glycolysis stress ECAR values, cell mitochondrial stress OCR (D) and ATP Rate OCR (E) of cells after the addition of different drugs. Compared to other groups, \*P<0.05. (F) Difference in glucose uptake capacity of cells after treatment with different drugs, \*P<0.05.

The role of the AKT/NF-kB signaling pathway axis in resistance to doxorubicin in vivo

In vivo validation was performed using a subcutaneous xenograft model in BALB/c nude mice. SUDHL8R cells were mixed with Matrigel and implanted, and once tumors reached\~100 mm³ (three weeks post-implantation), mice were treated for 10 days as follows: saline (control), doxorubicin alone (Dox), doxorubicin plus AKT inhibitor (Dox + AKT in), or doxorubicin plus NF-κB inhibitor (Dox + NF-κB in), with dosages

adjusted to body weight (**Figure 6A**). Body weight remained stable in controls but declined modestly in all treatment groups, mirroring clinical chemotherapy effects. Tumor volume increased progressively in controls but showed only a slight reduction with Dox alone; in contrast, both Dox + AKT in and Dox + NF-kB in groups exhibited robust tumor growth inhibition (**Figure 6B**). Final tumor weights confirmed significant suppression by combination therapy (\*P<0.05, **Figure 6C**), and H&E staining verified tumor integrity (**Figure 6D**). Western blotting

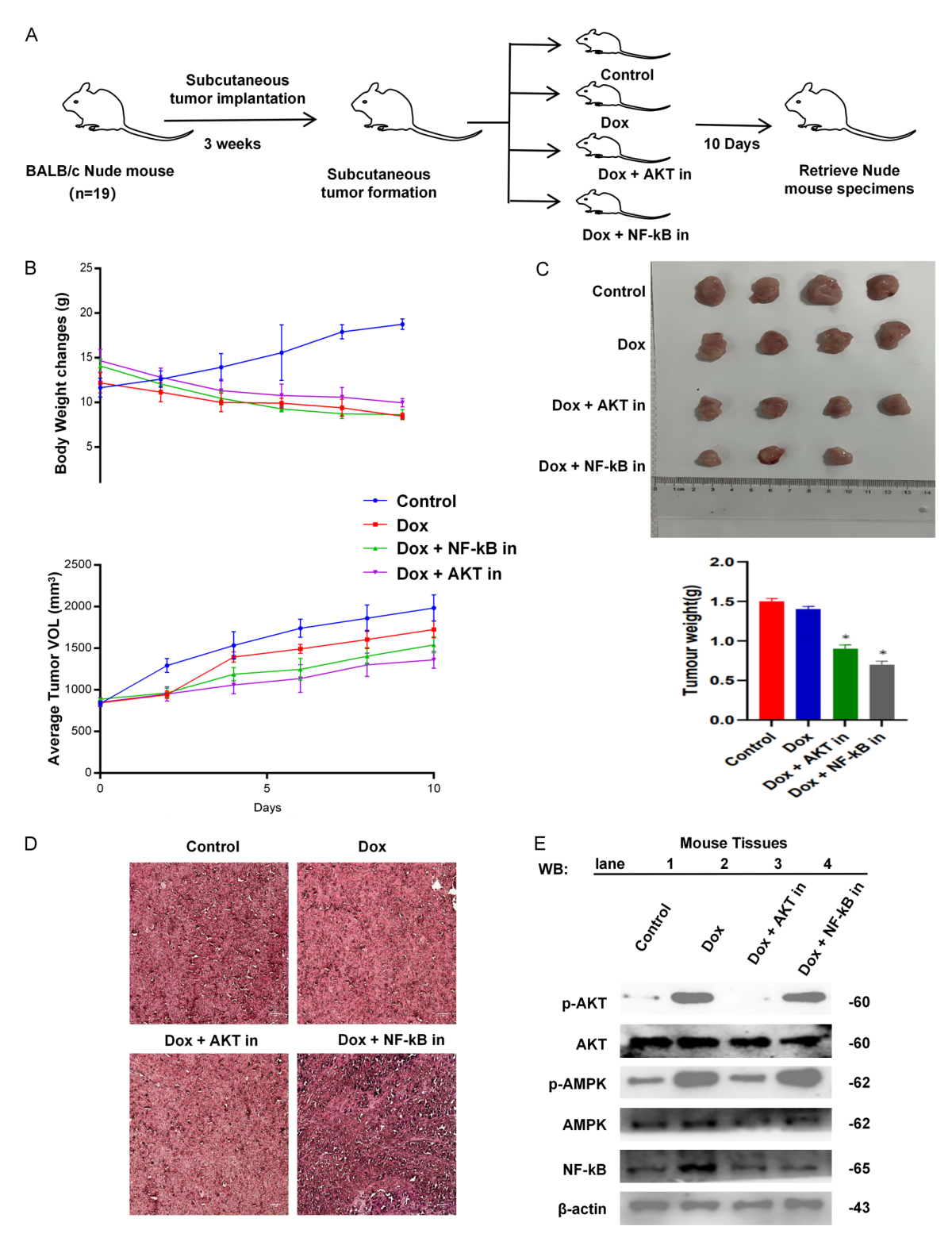


Figure 6. Validation of the regulatory effect of the AKT/NF-κB signaling pathway axis on cell resistance *in vivo*. A. Diagram of the animal experimental model. B. Graph showing changes in body weight and tumor volume of mice after treatment. C. Comparative image of tumors extracted from euthanized nude mice. Compared to Control and Dox groups, \*P<0.05. D. H&E staining of tumor samples (×400). E. Western Blot analysis of key proteins in the AKT, AMPK, and NF-κB signaling pathways in tumor tissues.

revealed that AKT inhibition not only reduced phospho-AKT levels but also decreased AMPK phosphorylation and downstream NF-κB activation, whereas NF-κB inhibition selectively blocked NF-κB without affecting upstream AKT or AMPK (Figure 6E). These results corroborate that dysregulated AKT/AMPK-NF-κB signaling drives doxorubicin resistance in DLBCL and that dual targeting of these pathways can effectively reverse chemoresistance.

# Discussion

Resistance to doxorubicin in DLBCL arises from tumor cell subpopulations that possess intrinsic or acquired defenses against chemotherapeutic stress. Upon exposure to doxorubicin, these resistant cells mount a unique transcriptional program that dysregulates key metabolic pathways - most notably the AKT and downstream NF-kB signaling axes - ultimately reprogramming glucose metabolism to support survival.

Numerous studies across cancer types have implicated NF-κB as a central mediator of chemoresistance [35, 36], and aberrant NF-κB activation is especially prevalent in refractory DLBCL patients [37]. However, the upstream metabolic drivers of NF-κB in DLBCL remain poorly defined. Here, we introduce AKT - a master regulator of glucose uptake and glycolysis as a critical modulator of NF-κB signaling. Recent work in prostate cancer demonstrates that hyperactive AKT enhances NF-κB-driven drug resistance [38], suggesting a conserved mechanism worthy of investigation in DLBCL.

Consistent with this model, we observed that doxorubicin-resistant DLBCL cells display markedly increased glycolytic capacity. This shift mirrors a broader phenomenon in which cancer cells, under prolonged chemotherapeutic pressure, rewire their metabolism - particularly glucose metabolism - to rapidly generate ATP and biosynthetic precursors for survival [39]. Indeed, elevated lactate production has been reported in drug-resistant DLBCL lines, further linking glycolysis to chemoresistance [14].

While our data highlight the AKT/NF-kB axis, other oncogenic pathways - such as Wnt signaling - may also contribute. Doxorubicin-induced upregulation of FZD1 and WNT10A can establish an autocrine Wnt loop, which not only sus-

tains cancer stem-like properties but also intersects with NF-kB to drive metabolic adaptation and therapy resistance [40-42]. Whether Wnt activity converges on AKT to reinforce glycolytic reprogramming deserves future study. Likewise, our preliminary observations of AMPK activation in resistant cells raise intriguing questions about cross-talk between energy sensing and survival signaling.

In summary, we demonstrate that aberrant AKT activity reprograms glucose metabolism and amplifies NF-kB signaling to promote doxorubicin resistance in DLBCL. These findings not only elucidate a metabolic basis for chemoresistance but also suggest that targeting the AKT/NF-kB axis - or its metabolic circuitry - may offer novel therapeutic strategies for refractory DLBCL.

# Acknowledgements

The projects received support from the Excellent Doctoral Research Start-up Fund of the First Hospital of Lanzhou University (Idyyyn2019-06), Lanzhou Science and Technology Plan Project (2020-ZD-68).

# Disclosure of conflict of interest

None.

Address correspondence to: Ya-Ming Xi, Department of Hematology, The First Hospital, Lanzhou University, No. 1 Donggang West Road, Chengguan District, Lanzhou 730000, Gansu, P. R. China. Fax: +86-0931-8619797; E-mail: xiyaming02@163.com; Qi-Yu Feng, Cancer Research Center, The First Affliliated Hospital of USTC, Division of Life Sciences and Medicine, University of Science and Technology of China, Hefei 230036, Anhui, P. R. China. Tel: +86-0551-63607040; E-mail: qiyufeng@ustc.edu.cn

### References

- [1] Li S, Young KH and Medeiros LJ. Diffuse large B-cell lymphoma. Pathology 2018; 50: 74-87.
- [2] Poletto S, Novo M, Paruzzo L, Frascione PMM and Vitolo U. Treatment strategies for patients with diffuse large B-cell lymphoma. Cancer Treat Rev 2022; 110: 102443.
- [3] Susanibar-Adaniya S and Barta SK. 2021 Update on Diffuse large B cell lymphoma: a review of current data and potential applications on risk stratification and management. Am J Hematol 2021; 96: 617-629.

- [4] Goldfinger M and Cooper DL. Refractory DLB-CL: challenges and treatment. Clin Lymphoma Myeloma Leuk 2022; 22: 140-148.
- [5] Lu X, Zhang Q and Xie Y. TCFL5 knockdown sensitizes DLBCL to doxorubicin treatment via regulation of GPX4. Cell Signal 2023; 110: 110831.
- [6] Gini G, Tani M, Tucci A, Marcheselli L, Cesaretti M, Bellei M, Pascarella A, Ballerini F, Petrini M, Merli F, Olivieri A, Lanza F, Annibali O, Zilioli VR, Liberati AM, Tisi MC, Arcari A, Marino D, Musuraca G, Pavone V, Fabbri A, Pozzi S, Mannina D, Plenteda C, Celli M and Luminari S. Lenalidomide plus rituximab for the initial treatment of frail older patients with DLBCL: the FIL\_ReRi phase 2 study. Blood 2023; 142: 1438-1447.
- [7] Zhang J, Gu Y and Chen B. Drug-resistance mechanism and new targeted drugs and treatments of relapse and refractory DLBCL. Cancer Manag Res 2023; 15: 245-255.
- [8] Guo L, Lin P, Xiong H, Tu S and Chen G. Molecular heterogeneity in diffuse large B-cell lymphoma and its implications in clinical diagnosis and treatment. Biochim Biophys Acta Rev Cancer 2018; 1869: 85-96.
- [9] Karmali R and Gordon LI. Molecular subtyping in diffuse large B cell lymphoma: closer to an approach of precision therapy. Curr Treat Options Oncol 2017; 18: 11.
- [10] Pranzini E, Pardella E, Paoli P, Fendt SM and Taddei ML. Metabolic reprogramming in anticancer drug resistance: a focus on amino acids. Trends Cancer 2021; 7: 682-699.
- [11] Ricci JE and Chiche J. Metabolic reprogramming of non-Hodgkin's B-cell lymphomas and potential therapeutic strategies. Front Oncol 2018; 8: 556.
- [12] Pi M, Kuang H, Yue C, Yang Q, Wu A, Li Y, Assaraf YG, Yang DH and Wu S. Targeting metabolism to overcome cancer drug resistance: a promising therapeutic strategy for diffuse large B cell lymphoma. Drug Resist Updat 2022; 61: 100822.
- [13] Bhalla K, Jaber S, Nahid M N, Underwood K, Beheshti A, Landon A, Bhandary B, Bastian P, Evens AM, Haley J, Polster B and Gartenhaus RB. Role of hypoxia in diffuse large B-cell lymphoma: metabolic repression and selective translation of HK2 facilitates development of DLBCL. Sci Rep 2018; 8: 744.
- [14] Lim SK, Peng CC, Low S, Vijay V, Budiman A, Phang BH, Lim JQ, Jeyasekharan AD, Lim ST, Ong CK, Tan SM and Li Y. Sustained activation of non-canonical NF-κB signalling drives glycolytic reprogramming in doxorubicin-resistant DLBCL. Leukemia 2023; 37: 441-452.
- [15] Curtis NJ, Mooney L, Hopcroft L, Michopoulos F, Whalley N, Zhong H, Murray C, Logie A, Revill M, Byth KF, Benjamin AD, Firth MA, Green S,

- Smith PD and Critchlow SE. Pre-clinical pharmacology of AZD3965, a selective inhibitor of MCT1: DLBCL, NHL and Burkitt's lymphoma anti-tumor activity. Oncotarget 2017; 8: 69219-69236.
- [16] Tinajero MG and Malik VS. An update on the epidemiology of type 2 diabetes: a global perspective. Endocrinol Metab Clin North Am 2021; 50: 337-355.
- [17] Tsilidis KK, Kasimis JC, Lopez DS, Ntzani EE and Ioannidis JP. Type 2 diabetes and cancer: umbrella review of meta-analyses of observational studies. BMJ 2015; 350: g7607.
- [18] Tanase DM, Gosav EM, Costea CF, Ciocoiu M, Lacatusu CM, Maranduca MA, Ouatu A and Floria M. The Intricate Relationship between Type 2 Diabetes Mellitus (T2DM), Insulin Resistance (IR), and Nonalcoholic Fatty Liver Disease (NAFLD). J Diabetes Res 2020; 2020: 3920196.
- [19] Demir S, Nawroth PP, Herzig S and Ekim Üstünel B. Emerging targets in type 2 diabetes and diabetic complications. Adv Sci (Weinh) 2021; 8: e2100275.
- [20] Schlesser C, Meul T, Stathopoulos G and Meiners S. Metformin induces resistance of cancer cells to the proteasome inhibitor bortezomib. Biomolecules 2022; 12: 756.
- [21] Zhang H, Yu J, Ma L, Zhao Y, Xu S, Shi J, Qian K, Gu M, Tan H, Xu L, Liu Y, Mu C and Xiong Y. Reversing multi-drug resistance by polymeric metformin to enhance antitumor efficacy of chemotherapy. Int J Pharm 2022; 624: 121931.
- [22] Park JY, Lee GH, Yoo KH and Khang D. Overcoming multidrug-resistant lung cancer by mitochondrial-associated ATP inhibition using nanodrugs. J Nanobiotechnology 2023; 21: 12.
- [23] Song J, Liu J, Cui C, Hu H, Zang N, Yang M, Yang J, Zou Y, Li J, Wang L, He Q, Guo X, Zhao R, Yan F, Liu F, Hou X, Sun Z and Chen L. Mesenchymal stromal cells ameliorate diabetes-induced muscle atrophy through exosomes by enhancing AMPK/ULK1-mediated autophagy. J Cachexia Sarcopenia Muscle 2023; 14: 915-929.
- [24] Xie Z, Wang X, Luo X, Yan J, Zhang J, Sun R, Luo A and Li S. Activated AMPK mitigates diabetesrelated cognitive dysfunction by inhibiting hippocampal ferroptosis. Biochem Pharmacol 2023; 207: 115374.
- [25] Li H, Song D, Liu Q, Li L, Sun X, Guo J, Li D and Li P. miR-351 promotes atherosclerosis in diabetes by inhibiting the ITGB3/PIK3R1/Akt pathway and induces endothelial cell injury and lipid accumulation. Mol Med 2022; 28: 120
- [26] Ramasubbu K and Devi Rajeswari V. Impairment of insulin signaling pathway PI3K/Akt/

- mTOR and insulin resistance induced AGEs on diabetes mellitus and neurodegenerative diseases: a perspective review. Mol Cell Biochem 2023: 478: 1307-1324.
- [27] Rabah HM, Mohamed DA, Mariah RA, Abd El-Khalik SR, Khattab HA, AbuoHashish NA, Abdelsattar AM, Raslan MA, Farghal EE and Eltokhy AK. Novel insights into the synergistic effects of selenium nanoparticles and metformin treatment of letrozole induced polycystic ovarian syndrome: targeting PI3K/Akt signalling pathway, redox status and mitochondrial dysfunction in ovarian tissue. Redox Rep 2023; 28: 2160569.
- [28] Shearer AM, Wang Y, Fletcher EK, Rana R, Michael ES, Nguyen N, Abdelmalek MF, Covic L and Kuliopulos A. PAR2 promotes impaired glucose uptake and insulin resistance in NAFLD through GLUT2 and Akt interference. Hepatology 2022; 76: 1778-1793.
- [29] Ji A, Chen W, Liu C, Zhang T, Shi R, Wang X, Xu H and Li D. Soy protein compared with whey protein ameliorates insulin resistance by regulating lipid metabolism, AMPK/mTOR pathway and gut microbiota in high-fat diet-fed mice. Food Funct 2023; 14: 5752-5767.
- [30] Ren G, Ma Y, Wang X, Zheng Z and Li G. Aspirin blocks AMPK/SIRT3-mediated glycolysis to inhibit NSCLC cell proliferation. Eur J Pharmacol 2022; 932: 175208.
- [31] Xu P, Zheng Y, Liao J, Hu M, Yang Y, Zhang B, Kilby MD, Fu H, Liu Y, Zhang F, Xiong L, Liu X, Jin H, Wu Y, Huang J, Han T, Wen L, Gao R, Fu Y, Fan X, Qi H, Baker PN and Tong C. AMPK regulates homeostasis of invasion and viability in trophoblasts by redirecting glucose metabolism: Implications for pre-eclampsia. Cell Prolif 2023; 56: e13358.
- [32] Wei L, Zhou Q, Tian H, Su Y, Fu GH and Sun T. Integrin β3 promotes cardiomyocyte proliferation and attenuates hypoxia-induced apoptosis via regulating the PTEN/Akt/mTOR and ERK1/2 pathways. Int J Biol Sci 2020; 16: 644-654.
- [33] Li Y, Xia J, Jiang N, Xian Y, Ju H, Wei Y and Zhang X. Corin protects H2O2-induced apoptosis through PI3K/AKT and NF-κB pathway in cardiomyocytes. Biomed Pharmacother 2018; 97: 594-599.

- [34] Huang XY, Hu QP, Shi HY, Zheng YY, Hu RR and Guo Q. Everolimus inhibits Pl3K/Akt/mTOR and NF-kB/IL-6 signaling and protects seizure-induced brain injury in rats. J Chem Neuroanat 2021; 114: 101960.
- [35] Meng Q, Liang C, Hua J, Zhang B, Liu J, Zhang Y, Wei M, Yu X, Xu J and Shi S. A miR-146a-5p/TRAF6/NF-kB p65 axis regulates pancreatic cancer chemoresistance: functional validation and clinical significance. Theranostics 2020; 10: 3967-3979.
- [36] Jiang XM, Xu YL, Yuan LW, Zhang LI, Huang MY, Ye ZH, Su MX, Chen XP, Zhu H, Ye RD and Lu JJ. TGFβ2-mediated epithelial-mesenchymal transition and NF-κB pathway activation contribute to osimertinib resistance. Acta Pharmacol Sin 2021; 42: 451-459.
- [37] Turturro F. Constitutive NF-kB activation underlines major mechanism of drug resistance in relapsed refractory diffuse large B cell lymphoma. Biomed Res Int 2015; 2015; 484537.
- [38] Torrealba N, Vera R, Fraile B, Martínez-Onsurbe P, Paniagua R and Royuela M. TGF-β/Pl3K/AKT/mTOR/NF-kB pathway. Clinicopathological features in prostate cancer. Aging Male 2020; 23: 801-811.
- [39] Bhattacharya B, Mohd Omar MF and Soong R. The Warburg effect and drug resistance. Br J Pharmacol 2016; 173: 970-979.
- [40] Long X, Hu Y, Duan S, Liu X, Huang W, Liu X, Xu Q, Song W and Zhou J. MRGBP promotes colorectal cancer metastasis via DKK1/Wnt/β-catenin and NF-kB/p65 pathways mediated EMT. Exp Cell Res 2022; 421: 113375.
- [41] Du Q and Geller DA. Cross-regulation between Wnt and NF-κB signaling pathways. For Immunopathol Dis Therap 2010; 1: 155-181.
- [42] Duchartre Y, Kim YM and Kahn M. The Wnt signaling pathway in cancer. Crit Rev Oncol Hematol 2016; 99: 141-149.

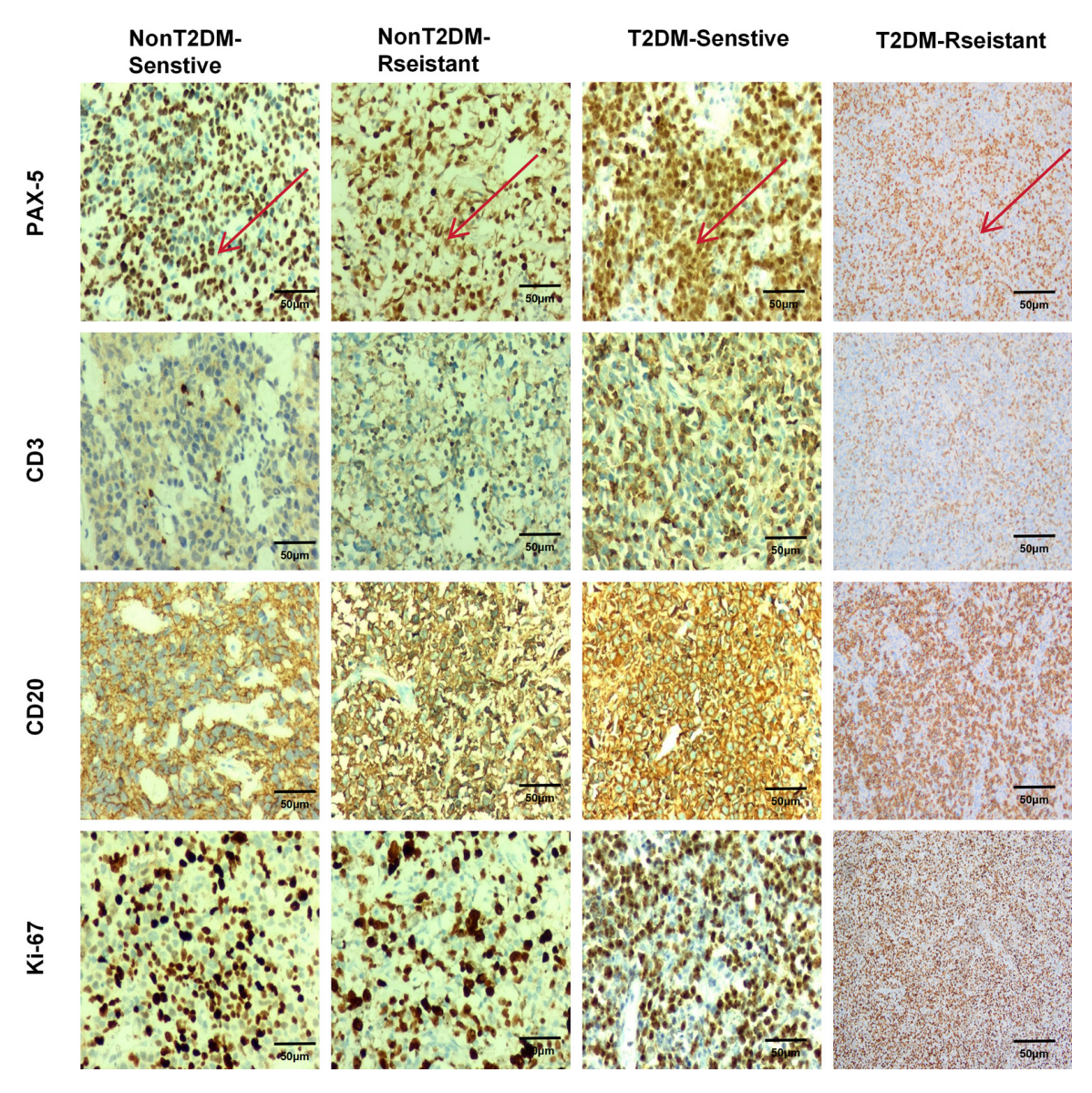


**Figure S1.** Immunohistochemical images of four groups of patients with confirmed diagnosis (PAX-5, CD3, CD20, Ki-67) (×200).

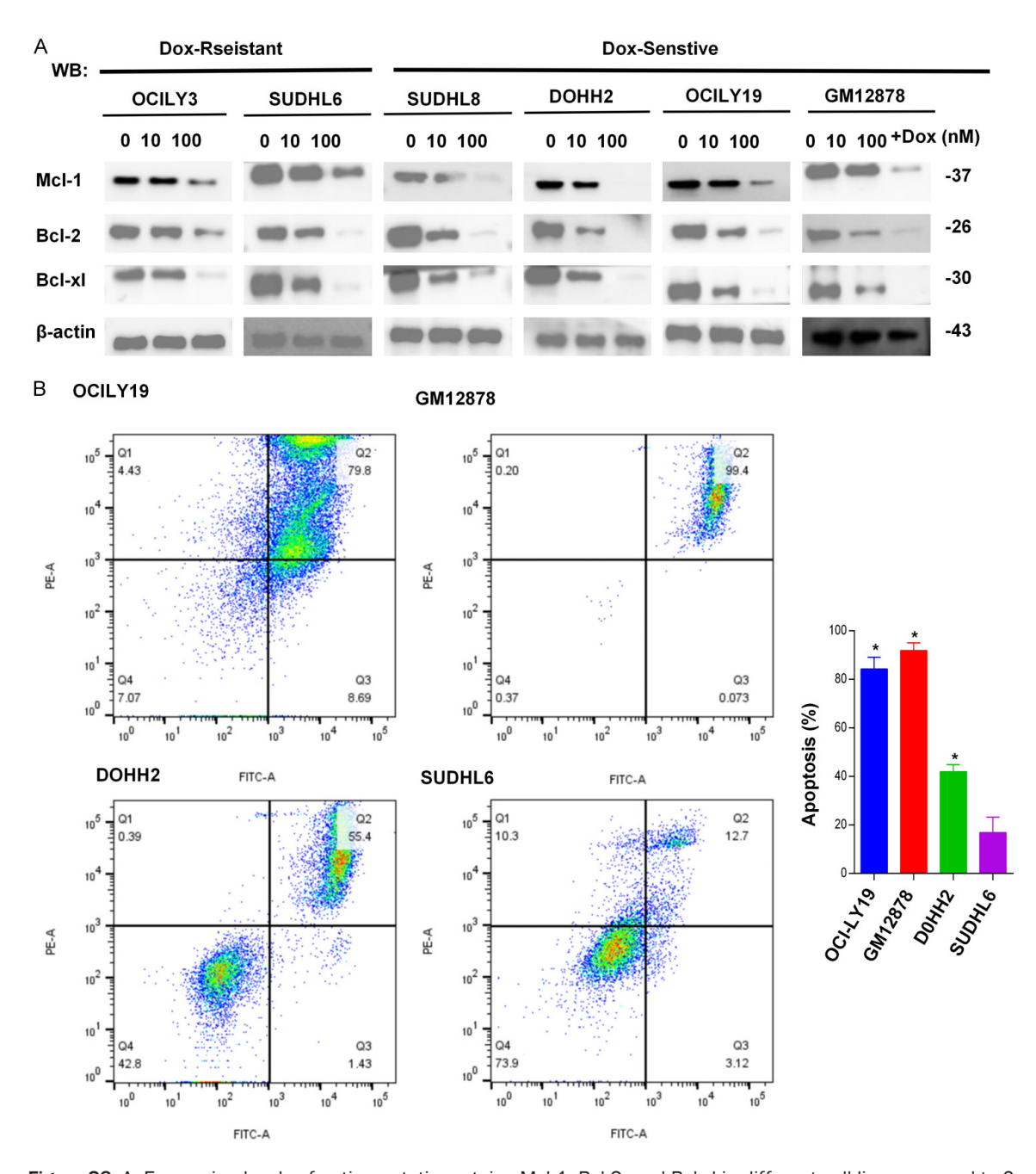


**Figure S2**. A. Expression levels of anti-apoptotic proteins Mcl-1, Bcl-2, and Bcl-xl in different cell lines exposed to 0, 10, and 100 nM Dox for 24 h. B. Apoptosis rate of sensitive cell line OCILY19, DOHH2, and resistant cell line SUDHL6, as well as normal B cell GM128 after 24 h of Doxorubicin treatment. Compared to SUDHL6 group, \*P<0.05.

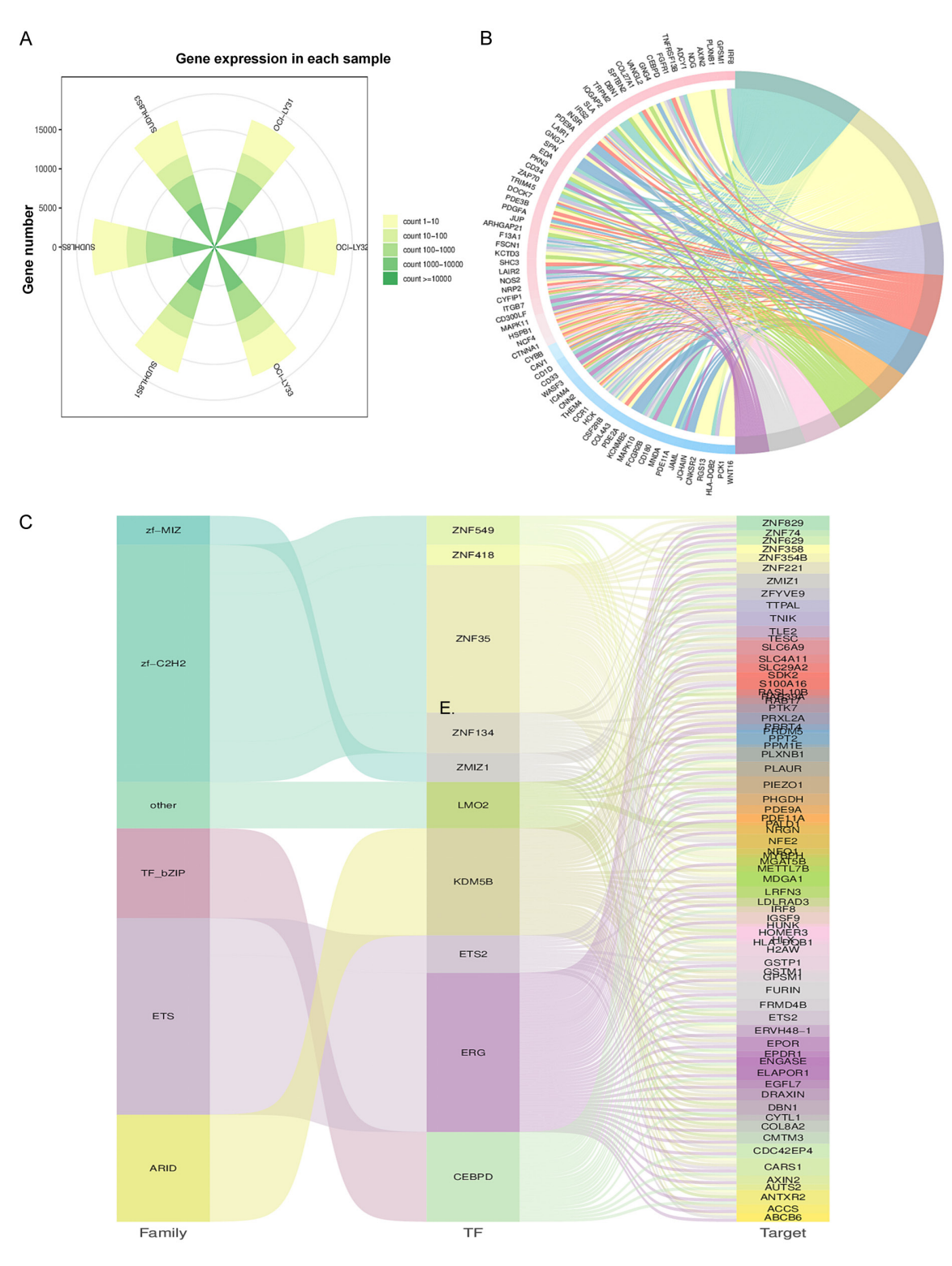


**Figure S3.** A. Quality control of proteomics samples for submission. B. Enrichment pathways of differential genes. C. Enriched gene families generated by gene enrichment pathways.

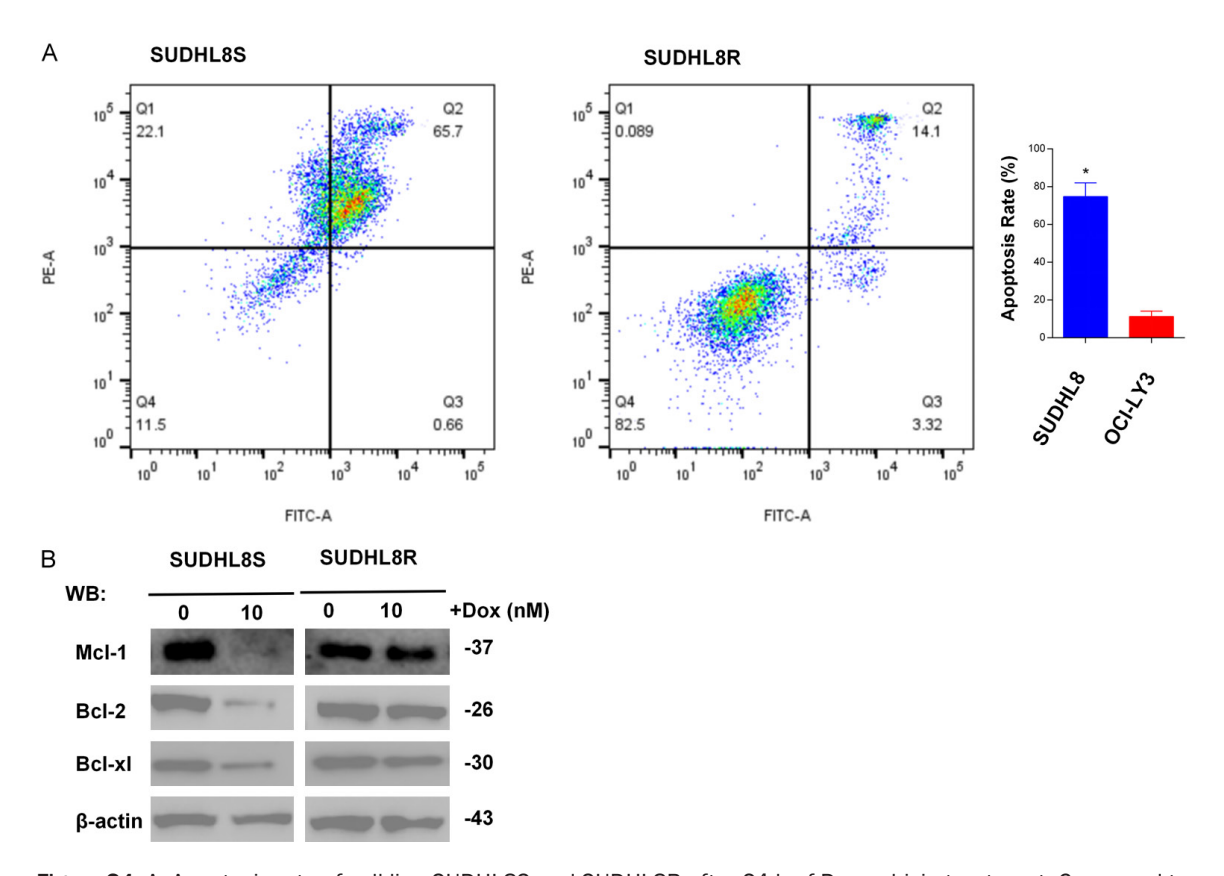


**Figure S4.** A. Apoptosis rate of cell line SUDHL8S and SUDHL8R after 24 h of Doxorubicin treatment. Compared to SUDHLR group, \*P<0.05. B. Expression levels of anti-apoptotic proteins McI-1, BcI-2, and BcI-xI in SUDHL8S and SUDHL8R exposed to 0, 10, and 100 nM Dox for 24 h.

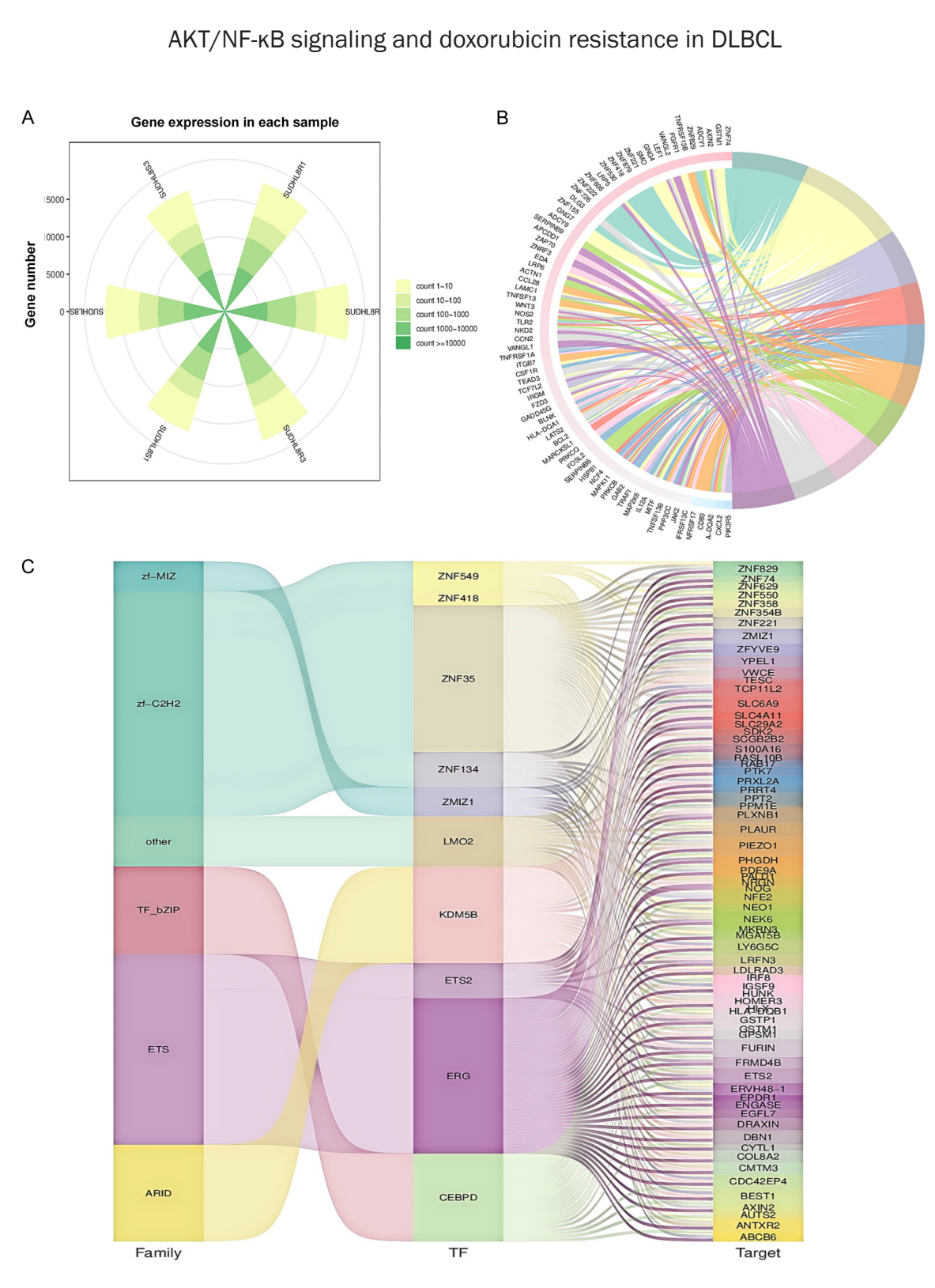


Figure S5. A. Quality control of proteomics samples for submission. B. Enrichment pathways of differential genes. C. Enriched gene families generated by gene enrichment pathways.

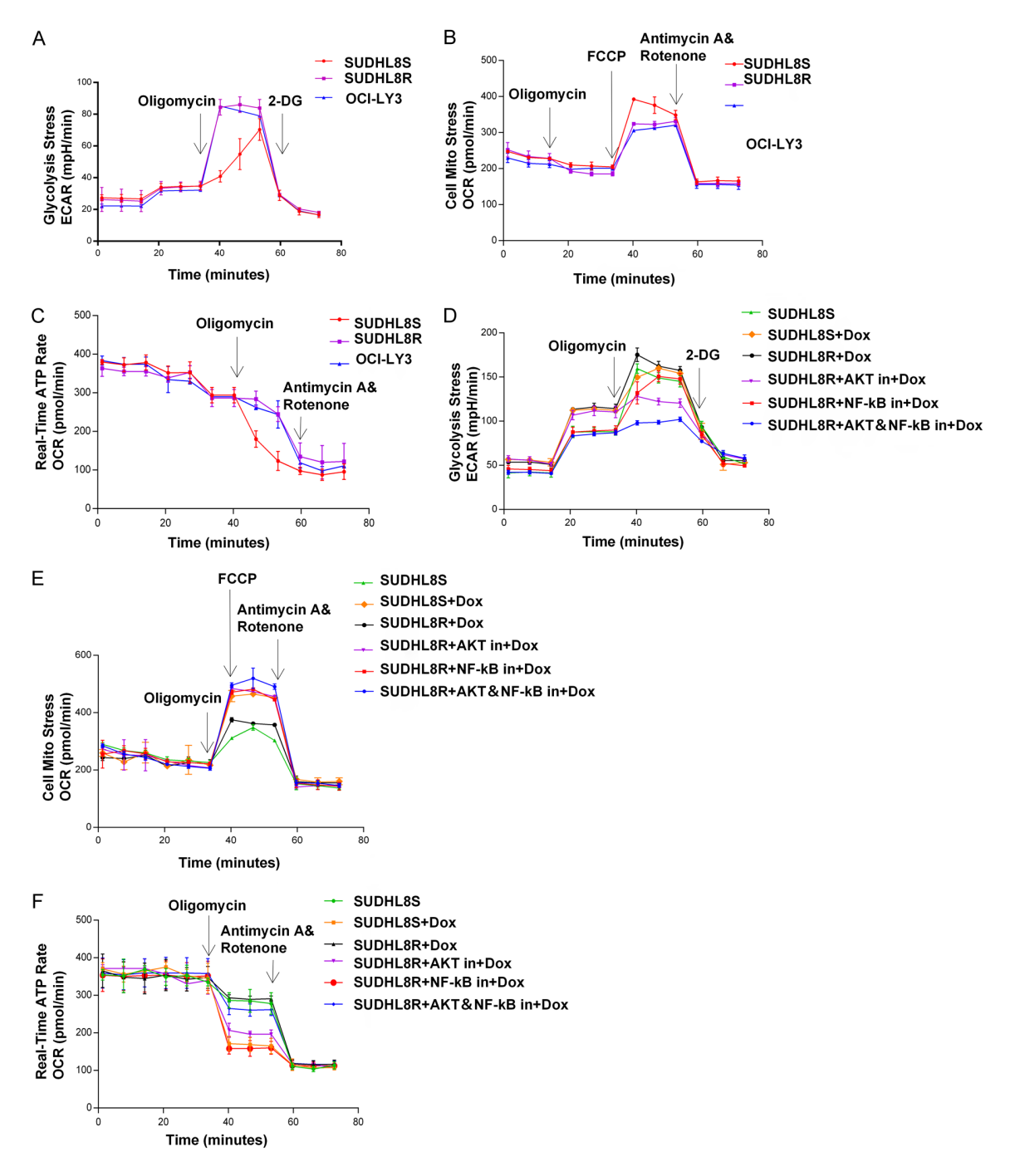


Figure S6. The values of glycolysis stress ECAR (A), cell mitochondrial stress OCR (B), and Real-Time ATP Rate OCR (C) detected in real-time for drug-resistant cells SUDHL8R, OCILY3, and sensitive cells SUDHL8S. The values of glycolysis stress ECAR (D), cell mitochondrial stress OCR (E), and Real-Time ATP Rate OCR (F) detected in real-time for six groups of cells under different drug treatments.

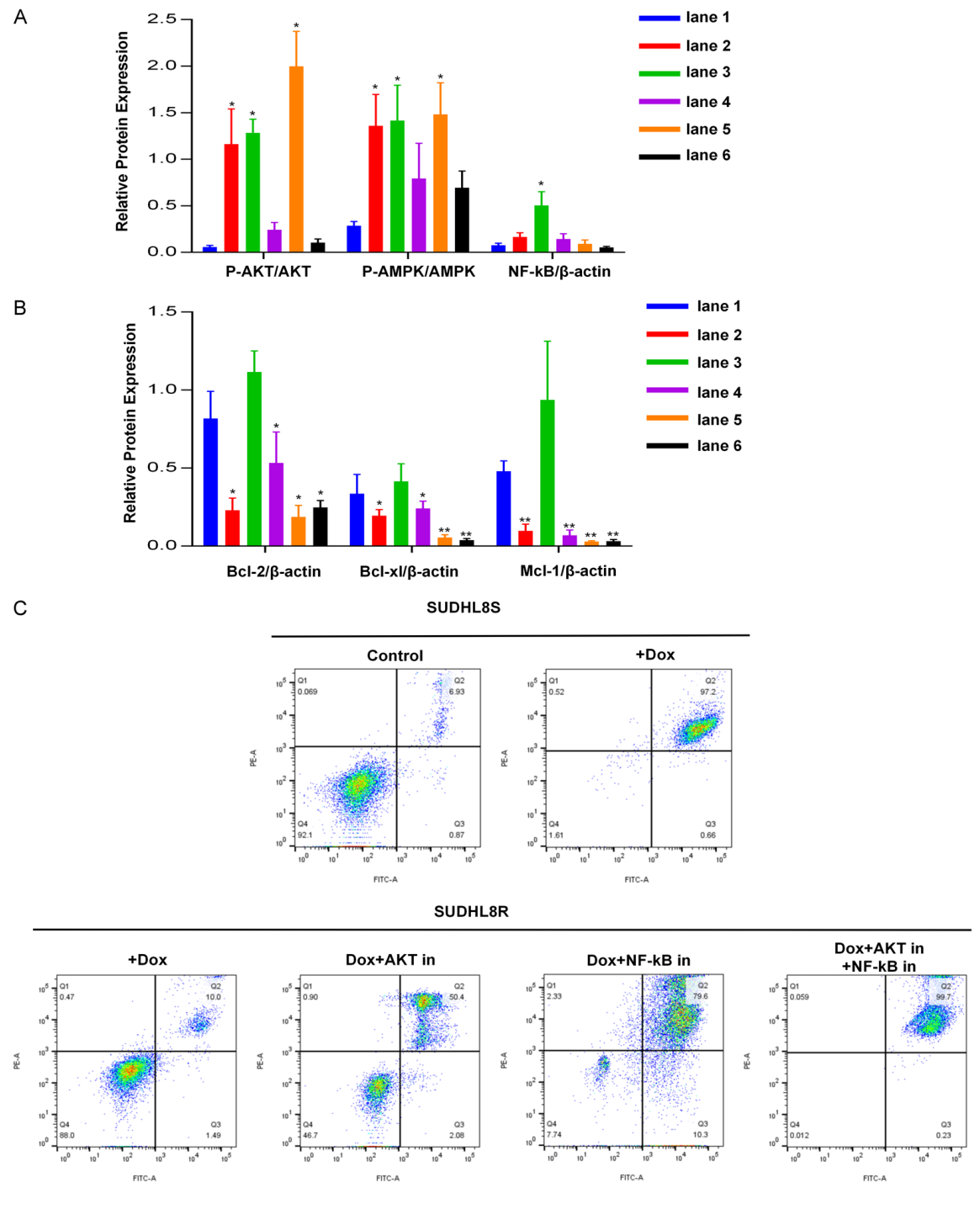


Figure S7. A. Quantitative analysis of the expression of AKT, AMPK, and NF-κB signaling pathway proteins after using inhibitors. B. Quantitative analysis of the expression of anti-apoptotic molecules after using inhibitors. C. Flow cytometry analysis to detect the differences in cell apoptosis after the addition of different drugs.